Paper accepted to Journal of Computational Physics

A novel pressure-velocity formulation and solution method for fluid-structure-interaction problems

Dr. George Papadakis
Department of Mechanical Engineering
King's College London,
WC2R, 2LS, London, UK.

Email: george.papadakis@kcl.ac.uk
tel: (+44)-020-7848209, fax: (+44)-020-7848-2932

Abstract

In the standard approach for simulating fluid-structure interaction problems the solution of the set of equations for solids provides the three displacement components while the solution of equations for fluids provides the three velocity components and pressure. In the present paper a novel reformulation of the elastodynamic equations for Hookean solids is proposed so that they contain the same unknowns as the Navier-Stokes equations, namely velocities and pressure. A separate equation for pressure correction is derived from the constitutive equation of the solid material. The system of equations for both media is discretised using the same method (finite volume on collocated grids) and the same iterative technique (SIMPLE algorithm) is employed for the pressure-velocity coupling. With this approach, the continuity of the velocity field at the interface is automatically satisfied. A special pressure correction procedure that enforces the compatibility of stresses at the interface is also developed. The new method is employed for the prediction of pressure wave propagation in an elastic tube. Computations were carried out with different meshes and time steps and compared with available analytic solutions as well as with numerical results obtained using the Flügge equations that describe the deformation of thin shells. For all cases examined the method showed very good performance.

Keywords: flow-structure interaction, finite volume method, SIMPLE algorithm, elastodynamic equations, flexible tube, pressure wave propagation.

1. Introduction

Fluid-structure interaction (FSI) is encountered in many areas of engineering (aerospace, civil or mechanical) as well as other scientific disciplines including medicine, biomechanics etc. FSI analysis becomes crucial when the deformation of a fluid boundary, for example a vessel wall, can not be neglected. During this interaction, the pressure and the viscous stresses of the fluid act on the solid boundary and lead to structural deformations, which in turn affect the fluid flow and consequently the velocities, pressure and viscous stresses of the fluid. Thus the response of the system can only be determined if the coupled problem is solved. In the case of liquids, which are almost incompressible, even a small structural deformation can have a significant effect. For example, in the case of blood flow in arteries, which are extremely flexible, the wave speed is 200 times slower than in an equivalent rigid tube.

In the standard approach for simulating fluid-structure interaction problems, the solids equation are solved for the three components of displacement while the fluids equations provide the three velocity components and pressure. In this approach, the pressure and viscous stresses become the boundary conditions for the solid equations. These are then solved and from the calculated displacements a new computational domain is obtained in which the fluid equations are solved again. This is the fundamental concept of the so-called “partitioned” methods [1-5]. There are various approaches regarding the degree of coupling i.e. how often and when information is transferred from one medium to the other. For example in an implicitly (or fully) coupled approach, the exchange of information is repeated until both sets of equations converge to within a prescribed tolerance and only then is the procedure advanced to the next time step.

“Monolithic” approaches, in which the two components are discretised and

solved simultaneously, have also been developed. They employ almost exclusively the finite element method and rely on the solution of a large coupled system of equations with unknowns the velocity, pressure and displacement. For example, Bazilevs et al [6] solve the coupled system (obtained with Newton's method) iteratively with the GMRES procedure and simple diagonal scaling. Heil [7] examines the performance of other preconditioning techniques. Tezduyar et al [8] discuss the pros and cons of three coupling techniques (block-iterative, quasi-direct and direct coupling).

In order to derive a unified approach for fluid-structure interaction problems, two issues need to be resolved: common discretisation method and common solution algorithm. "Partitioned" methods usually employ the finite element method for solids and the finite volume method for fluids. "Monolithic" methods use almost exclusively the finite element method, as already mentioned.

Both discretisation methods have a common starting equation but differ on how the integration of this equation in the domain is carried out [9]. The Galerkin finite element method sets the weighting functions equal to the shape functions over a control volume and zero outside. This leads to volume integrals that are computed using an appropriate quadrature rule. The method is very well established, has sound mathematical formulation and has been used very successfully for structural as well as flow problems [10-12]. On the other hand, in the finite volume method, the weighting functions take the value of unity over a control volume and zero outside. This transforms the volume integrals to surface integrals and makes the method conservative i.e. the flux through a face shared by two adjacent control volumes is the same for both volumes [13]. This property makes the method very attractive for fluid flow and heat transfer simulations. It is still the most widely used method in the CFD community [14] but it has also been employed successfully for structural analysis problems. For

example, a finite volume approach with non-orthogonal cells for two-dimensional plane elastostatic problems is proposed in [15]. The method was later extended to handle incompressible materials in a formulation that includes displacement and pressure as independent variables [16]. Discretisation of the elastic solid mechanics equations in three dimensions on an unstructured grid using this method is presented in [13]. Fallah et al [17] extended the method to large deformations and showed that the results are comparable with the finite element method.

The solution algorithm is also usually different for the two media. The elastodynamic equations most often are solved implicitly i.e. the discretised equations are cast in matrix form with unknowns the three components of the displacement vector. A conjugate gradient solver with preconditioning is then employed for the solution of the linear system. On the other hand, the Navier-Stokes equations are typically solved using a pressure-correction method in a segregated manner i.e. each equation is solved separately for one unknown (for example a velocity component or pressure). The segregated solution method can naturally handle non-linearities and is by far the preferred method in computational fluid dynamics. It has also been used for structural analysis problems. For example Demirdžic et al [18] used the finite volume method and a segregated solution algorithm coupled with multigrid acceleration to derive benchmark solutions for 3 cases. In [19] a discretisation practice was proposed that provides rapid convergence for a segregated solution method.

In the context of fluid-structure interaction, several investigators have combined the finite volume method and the segregated solution approach. For example Greeshields et al [20] solved separately the solid equations for displacements and the fluid equations for velocity and pressure. The motion of the interface was accounted for but they reported convergence problems when the modulus of elasticity of the solid was

much smaller to the bulk modulus of the fluid. Ivankovic et al [21] used a very similar method to study the blood flow through an atherosclerotic artery but the mesh was fixed and did not observe stability problems. Greenshields and Weller [22] derived a velocity-pressure formulation to solve a set of momentum and continuity equations that governs both fluid and solid, with velocity and pressure being the unknown variables for both media. A phase function is used to differentiate between them while the equations are discretised and solved in a single domain. Karac [23] used both a displacement-velocity-pressure as well as a velocity-pressure formulation to study the drop impact of fluid-filled polyethylene containers.

The main objective of the paper is to develop a novel velocity-pressure formulation and solution method for fluid structure interaction problems. The equation for pressure in fluids is derived from the continuity equation (as it is customary) while for solids is derived from the constitutive equation of the solid material. The governing partial differential equations are solved using the same discretisation method and solution algorithm (finite volume and SIMPLE algorithm respectively). The paper is organised as follows: the first part (sections 2-5) deals with solids only (new reformulation of the equations in terms of velocity and pressure, associated boundary conditions and numerical solution method). The second part (section 6) deals with the coupling between fluid and structure and more specifically presents a novel pressure correction methodology that enforces the compatibility of stresses (force balance) at the interface. Results from the application of the method to wave propagation in a flexible tube are presented in section 7 while in the final section 8 the main contributions and findings of the paper are summarized.

2. Conservation equations for continuous media

The following set of equations describe continuous media and are thus valid for both solids and fluids [24-25]:

Continuity equation (mass conservation)

$$\frac{\partial \rho}{\partial t} + \frac{\partial \rho U_i}{\partial x_i} = 0 \tag{1}$$

Momentum equations (Newton's second law of motion in 3 Cartesian directions)

$$\frac{\partial \rho U_i}{\partial t} + \frac{\partial \rho U_i U_j}{\partial x_j} = \frac{\partial \sigma_{ij}}{\partial x_j} \tag{2}$$

In the above equations ρ is the density, U_i the velocity component in direction i and σ_{ij} the components of the stress tensor. This paper is concerned with small displacements only and therefore these equations are written in an Eulerian reference frame. The assumption of small deformations also simplifies the numerical simulations because the computational mesh remains fixed. For larger deformations an arbitrary Langrangian-Eulerian approach is necessary in which the fluid and structure meshes move, following the deformation of the solid.

The aforementioned partial differential equations, which are valid for both media as already mentioned, are expressed in terms of fluid and structure velocities. The difference lies in the constitutive relation for the stress tensor σ. In fluids it is expressed in terms of the rate of strain tensor (i.e. velocities) and pressure, while in solids it is a function of the strain tensor (i.e. displacements). More specifically, for a linear, viscous (or Newtonian) fluid, the elements of the stress tensor σ_{ij} are given by:

$$\sigma_{ij} = -\left(p + \frac{2}{3}\eta \frac{\partial U_k}{\partial x_k} \right) \delta_{ij} + \eta \left(\frac{\partial U_i}{\partial x_j} + \frac{\partial U_j}{\partial x_i} \right) \tag{3}$$

where η is the laminar viscosity of the fluid and p the pressure. For incompressible flow $\frac{\partial U_k}{\partial x_k} = 0$ (due to the continuity equation) and the first term inside the parenthesis on the right hand side contains only pressure. Substituting this expression to equation (2) the well known Navier-Stokes equations are obtained.

For a linear, isotropic, elastic solid, the generalized Hooke's law is

$$\sigma_{ij} = \lambda \varepsilon_v \delta_{ij} + 2\mu \varepsilon_{ij} \tag{4}$$

where λ and μ are the two Lamé coefficients and the strain tensor ε is defined by:

$$\varepsilon_{ij} = \frac{1}{2}\left(\frac{\partial D_i}{\partial x_j} + \frac{\partial D_j}{\partial x_i} \right) \tag{5}$$

where D_i are the components of the displacement vector in Cartesian coordinates. In equation 4, ε_v is called dilatation and is equal to the trace of the tensor ε (or the divergence of the displacement vector) i.e.

$$\varepsilon_v = tr(\varepsilon) = \frac{\partial D_k}{\partial x_k} \tag{6}$$

where tr(.) is the trace operator. The Lamé coefficients are related to the Young's modulus (E) and the Poisson ratio (ν) with the following expressions:

$$\begin{aligned} \lambda &= \frac{\nu E}{(1+\nu)(1-2\nu)} \\ \mu &= \frac{E}{2(1+\nu)} \end{aligned} \tag{7}$$

Substituting 5-6 into equation 4 we get:

$$\sigma_{ij} = \lambda \frac{\partial D_k}{\partial x_k} \delta_{ij} + \mu \left(\frac{\partial D_i}{\partial x_j} + \frac{\partial D_j}{\partial x_i} \right) \tag{8}$$

Equations 4 and 8 are not general as they can not be used for incompressible solids for which $\nu \to 0.5$. The reason is that the Lamé coefficient λ tends to infinity and the

dilatation tends to 0 so their product $\lambda \frac{\partial D_k}{\partial x_k}$ that appears on the right hand side of the previous equation is indeterminable. This leads to the node-locking problem for incompressible solid materials [10-11]. Note that there are many practical applications involving incompressible materials, for example wave propagation in human arteries [26]. This problem is resolved by treating solid pressure as a separate unknown variable. In solid mechanics pressure is defined as

$$p = -\frac{tr(\sigma)}{3} = -\frac{1}{3}\left(\sigma_{11} + \sigma_{22} + \sigma_{33}\right) \tag{9}$$

Using the definition of the bulk modulus K,

$$K = -\frac{dp}{dV/V} = \rho \frac{dp}{d\rho} \tag{10}$$

it can be easily shown that pressure is related to dilatation ε_v by:

$$p = -K \cdot \varepsilon_v \tag{11}$$

The bulk modulus K is related to the Lamé coefficients by

$$K = \lambda + \frac{2}{3}\mu = \frac{E}{3(1-2\nu)} \tag{12}$$

Introducing pressure into the constitutive equation 8 we get:

$$\sigma_{ij} = -\left(p + \frac{2}{3}\mu \frac{\partial D_k}{\partial x_k} \right)\delta_{ij} + \mu\left(\frac{\partial D_i}{\partial x_j} + \frac{\partial D_j}{\partial x_i} \right) \tag{13}$$

This expression is valid for both compressible and incompressible solids because all the variables have now finite values and therefore this form is very convenient for the development of a general algorithm. Note also the similarity between the two constitutive expressions for the stress tensor for fluids and solids (i.e. equations 3 and 13).

The additional unknown (pressure) is obtained from the following equation:

$$\frac{1}{K}p + \varepsilon_v = 0 \Rightarrow \frac{1}{K}p + \frac{\partial D_i}{\partial x_i} = 0 \tag{14}$$

which is a rearranged form of equation 11. However in 14, both terms $\frac{1}{K}p$ and $\frac{\partial D_i}{\partial x_i}$ have finite values when $\nu \to 0.5$ (and therefore $K \to \infty$). For incompressible materials pressure must be extracted from the equation

$$\varepsilon_v = 0 \Rightarrow \frac{\partial D_i}{\partial x_i} = 0 \tag{15}$$

It can be seen therefore that the role of pressure for incompressible solids is to drive the divergence of the displacement field to 0. This is very similar to the role of pressure for incompressible fluids; it drives the divergence of the velocity field to zero. Note also that equation 15 does not contain pressure as unknown, so it must be extracted. This is analogous to the problem of obtaining pressure from the continuity equation in incompressible fluids. The developed approach can be directly applied to incompressible solids as will be shown later.

Substituting equation 13 into equation 2, after some algebra and assuming that the Lamé coefficients are constant we get:

$$\frac{\partial \rho U_i}{\partial t} + \frac{\partial \rho U_j U_i}{\partial x_j} = -\left(1 + \frac{\mu}{3K}\right)\frac{\partial p}{\partial x_i} + \mu \frac{\partial^2 D_i}{\partial x_j^2} \tag{16}$$

Equation 16 is in a very useful form since it can be used for either compressible or incompressible solids and all terms have finite values. For incompressible solids $1 + \frac{\mu}{3K} \to 1$ because $\frac{1}{K} \to 0$ and μ remains finite. For small displacements, the convection term $\frac{\partial \rho U_i U_j}{\partial x_j}$ is very small compared to the transient term and is usually neglected. However, in the following sections, this term will be retained as it is important for the fluid equations. Equation 16 is supplemented by equation 14 as well as

the relationship between displacements and solid velocities. Therefore, the following system of equations describes the solid dynamics mathematically:

$$\begin{cases} \dfrac{\partial \rho U_i}{\partial t} + \dfrac{\partial \rho U_j U_i}{\partial x_j} = -\left(1 + \dfrac{\mu}{3K}\right)\dfrac{\partial p}{\partial x_i} + \mu \dfrac{\partial^2 D_i}{\partial x_j^2} & (a) \\ \dfrac{\partial D_i}{\partial t} = U_i & (b) \\ \dfrac{1}{K} p + \dfrac{\partial D_i}{\partial x_i} = 0 & (c) \end{cases} \tag{17}$$

The solid velocity is the time derivative of displacement and this is expressed mathematically with equation 17(b). The corresponding system for a weakly compressible fluid is:

$$\begin{cases} \dfrac{\partial \rho U_i}{\partial t} + \dfrac{\partial \rho U_j U_i}{\partial x_j} = -\dfrac{\partial p}{\partial x_i} - \dfrac{\partial}{\partial x_i}\left(\dfrac{2}{3}\eta \dfrac{\partial U_k}{\partial x_k}\right) + \dfrac{\partial}{\partial x_j}\left[\eta\left(\dfrac{\partial U_i}{\partial x_j} + \dfrac{\partial U_j}{\partial x_i}\right)\right] & (a) \\ \dfrac{\rho}{K}\dfrac{\partial p}{\partial t} + \dfrac{\partial \rho U_i}{\partial x_i} = 0 & (b) \end{cases} \tag{18}$$

where the definition of the bulk modulus of the fluid K was used to express the time derivative $\dfrac{\partial \rho}{\partial t}$ in the continuity equation 1 in terms of pressure as $\dfrac{\rho}{K}\dfrac{\partial p}{\partial t}$.

For incompressible solids, system 17 reduces to

$$\begin{cases} \dfrac{\partial \rho U_i}{\partial t} + \dfrac{\partial \rho U_j U_i}{\partial x_j} = -\dfrac{\partial p}{\partial x_i} + \mu \dfrac{\partial^2 D_i}{\partial x_j^2} & (a) \\ \dfrac{\partial D_i}{\partial t} = U_i & (b) \\ \dfrac{\partial D_i}{\partial x_i} = 0 & (c) \end{cases} \tag{19}$$

while the corresponding system for an incompressible flow with constant viscosity η is:

$$\begin{cases} \dfrac{\partial \rho U_i}{\partial t} + \dfrac{\partial \rho U_j U_i}{\partial x_j} = -\dfrac{\partial p}{\partial x_i} + \eta \dfrac{\partial^2 U_i}{\partial x_j^2} \quad (a) \\ \dfrac{\partial U_i}{\partial x_i} = 0 \qquad\qquad\qquad\qquad (b) \end{cases} \tag{20}$$

The similarity between systems 19 and 20 is obvious. Systems 17 and 18 are also similar; the difference lies in the constant coefficient of the pressure gradient term and the rest of the terms in the right hand side. However, this is not a major problem since these terms are generally treated as a source in the discretised form. Although the forms are similar, one should not forget that the system of equations for solids is energy conserving (i.e. there is no mechanism for energy dissipation). For fluids on the other hand, the viscous terms are energy dissipating.

3. A velocity-pressure formulation for solids

Since the two conservation laws for continuous media (equations 1 and 2) are written in terms of velocities, it makes sense to use velocities as dependent variables for both solids and fluids. Such an approach has an additional advantage for fluid-structure interaction problems, namely the continuity of velocity field at the interface is satisfied automatically.

Equation 17(a) contains already velocity and pressure in the left and right hand sides respectively. However, the second term on the right hand side is the Laplacian of displacement. Also 17(c) contains the divergence of displacement. The presence of displacement in 17(a,c) is not a major problem, because it is linked with velocity through 17(b). The system of the two equations 17(a,b) can be integrated in time with any time advancement method. In the present paper the second order trapezoidal rule (Crank Nicolson scheme) was selected for the time advancement between time instants (k) and (k+1) i.e.

$$\begin{cases} \rho\dfrac{U_i^{(k+1)}-U_i^{(k)}}{\Delta t}+\dfrac{\partial \rho U_j^{(k+1)}U_i^{(k+1)}}{\partial x_j}=\dfrac{1}{2}\left[-\left(1+\dfrac{\mu}{3K}\right)\dfrac{\partial p^{(k+1)}}{\partial x_i}+\mu\dfrac{\partial^2 D_i^{(k+1)}}{\partial x_j^2}\right] \\ +\dfrac{1}{2}\left[-\left(1+\dfrac{\mu}{3K}\right)\dfrac{\partial p^{(k)}}{\partial x_i}+\mu\dfrac{\partial^2 D_i^{(k)}}{\partial x_j^2}\right] & (a) \\ \dfrac{D_i^{(k+1)}-D_i^{(k)}}{\Delta t}=\dfrac{1}{2}\left(U_i^{(k)}+U_i^{(k+1)}\right) & (b) \\ \dfrac{1}{K}p^{(k+1)}+\dfrac{\partial D_i^{(k+1)}}{\partial x_i}=0 & (c) \end{cases} \quad (21)$$

Any time integration scheme could have been selected. Since the convection term is usually very small, temporal accuracy for this term is not important and therefore it is evaluated implicitly at time instant (k+1). Solving equation 21(b) for $D_i^{(k+1)}$ and substituting in 21(a,c) the following system of equations that contains as unknowns $U_i^{(k+1)}$ and $p^{(k+1)}$ is obtained:

$$\begin{cases} \rho\dfrac{U_i^{(k+1)}-U_i^{(k)}}{\Delta t}+\dfrac{\partial \rho U_j^{(k+1)}U_i^{(k+1)}}{\partial x_j}=\dfrac{\mu\cdot\Delta t}{4}\cdot\dfrac{\partial^2 U_i^{(k+1)}}{\partial x_j^2}-\dfrac{1}{2}\left(1+\dfrac{\mu}{3K}\right)\dfrac{\partial p^{(k+1)}}{\partial x_i} \\ +\dfrac{\mu}{2}\cdot\dfrac{\partial^2 D_i^{(k)}}{\partial x_j^2}+\dfrac{\mu\cdot\Delta t}{4}\dfrac{\partial^2 U_i^{(k)}}{\partial x_j^2}+\dfrac{1}{2}\left[-\left(1+\dfrac{\mu}{3K}\right)\dfrac{\partial p^{(k)}}{\partial x_i}+\mu\dfrac{\partial^2 D_i^{(k)}}{\partial x_j^2}\right] & (a) \\ \dfrac{2\rho}{K}\dfrac{p^{(k+1)}}{\Delta t}+\dfrac{\partial \rho U_i^{(k+1)}}{\partial x_i}=-\dfrac{2\rho}{\Delta t}\dfrac{\partial D_i^{(k)}}{\partial x_i}-\dfrac{\partial \rho U_i^{(k)}}{\partial x_i} & (b) \end{cases} \quad (22)$$

Apart from the pressure gradient and velocity Laplacian term at time instant (k+1), the rest of the terms in the right hand side of 22(a) as well as all the terms in the right hand side of 22(b) are known from the previous time step (k). This is the final set of equations for solids that must be solved iteratively to obtain $U_i^{(k+1)}$ and $p^{(k+1)}$.

It must be noted at this point that several papers in the literature [27-30] as well as the book of LeVeque [31] describe how the hyperbolic system of elastodynamic equations can be written in terms of velocities and stresses. In the 3D case there are nine unknowns, namely the three velocity components and the 6 independent components of the stress tensor (or equivalently the 6 strain components as there is a linear and

invertible stress-strain relationship for Hookean solids). Displacements themselves do not appear in the above systems as they have been converted to velocities by taking the time derivative of the constitutive stress-strain relationship. The resulting system is then solved using standard techniques suitable for hyperbolic systems such Godunov-type schemes or the method of characteristics. From the velocities, the displacements are then evaluated by integration. This is an elegant approach but it leads to a system with a large number of equations (9 for the 3D case) but also most importantly such an approach can not be easily coupled with the Navier-Stokes equations that describe the motion of fluids. The reason is that the stresses in Newtonian fluids are uniquely determined by the velocities and only one additional variable, pressure. This means that if the aforementioned formulations for solids are used to solve a coupled fluid-structure interaction problem, some variables (velocities) will be evaluated in the whole domain, but from the rest of the variables, others will be evaluated in fluid domain (pressure) and others in the solid domain (6 stress or strain components). There is no doubt that such approach can work but it can be quite cumbersome. Using the present approach, all four variables will be evaluated in the whole domain. Greenshields and Weller [22] have also proposed a velocity-pressure approach but the formulation of the momentum equation is different and pressure is extracted from the general continuity equation.

4. Boundary conditions for the velocity-pressure equations.

Having derived the system of partial differential equations that must be solved, the next step is the formulation of boundary conditions using velocities and pressure. There are two general types of boundary conditions for solids: prescribed displacement and prescribed traction. The implementation of these conditions for the momentum and pressure equations is described in the following sections:

4.1 Prescribed displacement at the boundary

The velocity at the boundary is obtained simply by differentiating with respect to time the prescribed displacement. This velocity can be used as Dirichlet condition for the numerical solution of equation 22(a). The correct value of displacement is also used for the evaluation of the terms of the right hand side of 22(a,b).

4.2 Prescribed traction at the boundary

Suppose that the prescribed traction is f_i. Then the force balance at the boundary is:

$$\sigma_{ij} n_j = f_i \tag{23}$$

where n_j are the components of the unit vector normal to the boundary and pointing outwards. Substituting equation 13 for σ_{ij} we get:

$$\left(-\left(p + \frac{2}{3}\mu \frac{\partial D_k}{\partial x_k} \right)\delta_{ij} + \mu\left(\frac{\partial D_i}{\partial x_j} + \frac{\partial D_j}{\partial x_i} \right) \right) n_j = f_i \tag{24}$$

This is a vector equation. Projecting this equation to the boundary normal vector $\vec{n}$ (i.e. taking the dot product with $\vec{n}$), we obtain:

$$n_i \left[\left(-\left(p + \frac{2}{3}\mu \frac{\partial D_k}{\partial x_k} \right)\delta_{ij} + \mu\left(\frac{\partial D_i}{\partial x_j} + \frac{\partial D_j}{\partial x_i} \right) \right) n_j \right] = n_i f_i \tag{25}$$

which after some algebra and employing equations 12 and 14 becomes:

$$-\frac{\lambda}{K} p + 2\mu \frac{\partial D_n}{\partial n} = n_i f_i \tag{26}$$

where $D_n = D_i n_i$ is the displacement in the direction normal to the boundary and $\frac{\partial}{\partial n}$ denotes derivative in that direction. Note that this equation can also be derived directly from 4 if both i and j are in the $\vec{n}$ direction. The ratio $\frac{\lambda}{K} = \frac{3\nu}{1+\nu}$ i.e. remains

finite so equation 26 is applicable for both compressible and incompressible solids. This is an equation that implicitly links the pressure and the normal component of displacement at the interface and will provide the boundary condition for the pressure equation as will be explained in the next section.

Two more scalar equations can be obtained by taking the dot product of equation 24 with tangential vectors τ_1 and τ_2. For example for vector τ_1 we get:

$$\mu\left(\frac{\partial D_{\tau_1}}{\partial n}+\frac{\partial D_n}{\partial \tau_1}\right)=\tau_{1_i} f_i \tag{27}$$

where $D_{\tau_1}=D_i\tau_{1_i}$ is the tangential component of displacement at the boundary in the direction τ_1. Again this equation could have been obtained directly from 4. A similar equation can be obtained for τ_2. Note that these equations do not contain pressure. They are used for the evaluation of D_{τ_1}, D_{τ_2} at the boundary. From the values of $D_n, D_{\tau_1}, D_{\tau_2}$ the displacement components in the Cartesian directions D_i can be easily evaluated.

5. Discretisation and solution algorithm.

The next step is the selection of discretisation and solution method of the reformulated set of partial differential equations that describe the solid behaviour. The selected discretisation method is the finite volume method while for the iterative solution of equations the SIMPLE algorithm is employed. This combination has been used successfully for decades in Computational Fluid Dynamics [14]. In fluid mechanics, the algorithm is employed to extract a pressure correction equation from the continuity equation. It will be used here to derive a pressure correction equation from 22(b).

In the following equations the time step indicator (k+1) is dropped on the understanding that the unknown variables U_i and p refer to this time step. The discretised momentum equations 22(a) can be written as:

$$A_P^{U_i} \cdot U_{i,P} = \sum_{nb} A_{nb}^{U_i} \cdot U_{i,nb} + S_{U_i} - \frac{1}{2}\left(1 + \frac{\mu}{3K}\right)\frac{\delta p}{\delta x_i}\Delta V \tag{28}$$

where P denotes the centroid of the control volume around which the equation is discretised and nb denotes the neighbouring points. S_{U_i} contains all the source terms (such as contributions from the previous time step (k) and non-orthogonality terms etc) apart from the contribution of the pressure gradient term that appears explicitly in the semi-discretised form $\frac{\delta p}{\delta x_i}$. Equations 28 are solved using a pressure field p* which generally will not be the correct one (it will be correct only at convergence within one time step) and therefore the resulting velocities (U_i^*) will not satisfy the discretised form of equation 22(b). So pressures and face velocities need to be corrected according to

$$\begin{aligned} p &= p^* + p' \\ U_n &= U_n^* + U_n' \end{aligned} \tag{29}$$

and these corrected values should satisfy the equation:

$$\frac{2\rho_P}{K}\frac{p_P^* + p_P'}{\Delta t} \cdot \Delta V + \sum_{face\ f}\left[\rho\left(U_n^* + U_n'\right)A\right]_f = S_m \tag{30}$$

where ΔV the volume of the computational cell. The term S_m on the right hand side is equal to $S_m = -\sum_{face\ f}\left(\frac{2\rho}{\Delta t}D_n A + \rho U_n A\right)_f$ and is known from the previous time step (k).

In the previous equations $U_n = U_i n_i$ and $D_n = D_i n_i$ are the velocity and displacement

components normal to the face. The face velocities U_n^* in equation 30 are evaluated using the Rhie and Chow [35] interpolation method:

$$U_n^* = \overline{U_n^*} - \frac{1}{2}\left(1+\frac{\mu}{3K}\right)\frac{\overline{\Delta V}}{A_P^{U_i}}\left(\frac{\delta p^*}{\delta n} - \overline{\frac{\delta p^*}{\delta n}}\right) \tag{31}$$

where an overbar denotes interpolation between the values of the centroids on either side of the face and $\frac{\delta(\,)}{\delta n}$ is the discrete approximation of the first order derivative normal to the boundary. The velocity corrections U_n' are related to pressure corrections p' with (for details in the case of fluids see [14, 32]):

$$U_n' = -\frac{1}{2}\left(1+\frac{\mu}{3K}\right)\frac{\overline{\Delta V}}{A_P^{U_i}}\frac{\delta p'}{\delta n} \tag{32}$$

Assuming that the mesh is orthogonal and the distance between the centroids P and nb is $\delta\xi$, U_n' can be written as:

$$U_n' = -\frac{1}{2}\left(1+\frac{\mu}{3K}\right)\frac{\overline{\Delta V}}{A_P^{U_i}}\frac{p'_{nb} - p'_P}{\delta\xi} \tag{33}$$

Extensions for non-orthogonal meshes are straightforward [33]. Substituting equation 33 into 30 the following equation for pressure correction is obtained

$$\frac{2\rho_P}{K}\frac{p_P^* + p'_P}{\Delta t}\cdot\Delta V + \sum_{face\ f}\left[\rho\left(U_n^* - \frac{1}{2}\left(1+\frac{\mu}{3K}\right)\frac{\overline{\Delta V}}{A_P^{U_i}}\frac{p'_{nb} - p'_P}{\delta\xi}\right)A\right]_f = S_m \tag{34}$$

The pressure, face velocities and face displacements are then corrected and the updated fields are used in the solution of the momentum equations in the next iteration. The face displacements D_n are calculated from 21(b) using the face velocity values i.e.

$$D_n = D_n^{(k)} + \frac{1}{2}\left(U_n^{(k)} + U_n\right)\Delta t \tag{35}$$

5.1 Implementation of boundary conditions

Within the context of the algorithm described above, the implementation of the prescribed displacement boundary condition is straightforward. However, the implementation of the prescribed traction boundary condition (equation 23) is more involved. The component normal to the boundary (equation 26) will be used to derive a Dirichlet boundary condition for the pressure correction equation. The boundary pressure (p_b^*) and normal displacement (D_n^*) must be corrected so as to satisfy equation 26 i.e.

$$-\frac{\lambda}{K}(p_b^* + p_b') + 2\mu\left(\frac{\delta D_n^*}{\delta n} + \frac{\delta D_n'}{\delta n}\right) = n_i f_i \tag{36}$$

Using equation 35, the displacement correction D_n' is evaluated from the pressure correction as:

$$D_n' = \frac{1}{2}U_n' \Delta t = -\frac{1}{4}\left(1 + \frac{\mu}{3K}\right)\frac{\overline{\Delta V}}{A_P^{U_i}}\frac{\delta p'}{\delta n}\Delta t \tag{37}$$

Substitution of the above equation in 36 yields an implicit equation that involves the 2nd order derivative of pressure correction at the boundary. The discretised form of this equation must then be solved for p_b'. However, approximation of higher order derivatives at boundaries is complicated especially in unstructured non-orthogonal meshes and solution for p_b' would result in a quite complicated expression. So it was decided to ignore the correction term $\frac{\delta D_n'}{\delta n}$ and obtain p_b' instead from:

$$-\frac{\lambda}{K}(p_b^* + p_b') + 2\mu\frac{\delta D_n^*}{\delta n} = n_i f_i \tag{38}$$

It must be noted that this type of approximation is very similar to the one employed by SIMPLE algorithm for the derivation of face velocity corrections (equation 32) as explained in [32]. In fact the PISO algorithm [34] was invented in order to remove this

deficiency of SIMPLE. Of course, a PISO-like approach can be used here as well and a second pressure correction equation can be derived that accounts for the neglected terms. It is important to stress that this approximation does not affect the final solution; it affects only the convergence rate. When the code has converged, all the corrections are zero and the equations are satisfied by the "starred" variables exactly. Solving for p_b' we have:

$$p_b' = -p_b^* - \frac{K}{\lambda}\left(n_i f_i - 2\mu \frac{\delta D_n^*}{\delta n} \right) \tag{39}$$

This is a Dirichlet condition for the boundary face value of pressure correction in equation 34. The derivative $\frac{\delta D_n^*}{\delta n}$ at the boundary is evaluated using a first order backward approximation.

6. Application to fluid-structure interaction problems.

The method is now ready to apply for the simulation of fluid-structure interaction problems. Two conditions must be satisfied at the interface: The solid and fluid velocity components are equal

$$U_{sj} = U_{fj} \tag{40}$$

and the total traction on the solid is due to the fluid pressure and viscous forces i.e. equation 23 becomes

$$\sigma_{ij} n_{sj} = (-p_f \cdot \delta_{ij} + t_{ij}) n_{sj} \tag{41}$$

where $t_{ij} = -\frac{2}{3}\eta \frac{\partial U_k}{\partial x_k}\delta_{ij} + \eta\left(\frac{\partial U_i}{\partial x_j} + \frac{\partial U_j}{\partial x_i} \right)$ is the viscous stress tensor and the vector $\vec{n}_s$ is shown in figure 1. The incorporation of these conditions on the discretised momentum and pressure correction equations is explained below.

6.1. Momentum equations

The first condition is automatically satisfied because velocity is a common variable for both media. Since the velocity field is continuous, the integration of the fluid and solid momentum equations in the F and S cells respectively presents no difficulty. For example the convection term $\frac{\partial \rho U_j U_i}{\partial x_j}$ is integrated as usual and any discretisation scheme can be used to approximate the face velocity (upwind, central, a bounded combination etc). The evaluation of the convective velocity is examined later because it is related directly to the calculation of pressure. It must be mentioned here that the diffusion term of the Navier-Stokes $\left(\eta \frac{\partial^2 U_i}{\partial x_j^2} \right)$ and the term $\frac{\mu \cdot \Delta t}{2} \cdot \frac{\partial^2 U_i}{\partial x_j^2}$ in the solids equations are evaluated separately in the corresponding cells. In other words the value of η and $\frac{\mu \cdot \Delta t}{2}$ in the centroids F and S respectively are not interpolated to find a value at the interface. The integration of the diffusive terms in the moving wall gives the shear stress, which for laminar flows can be evaluated directly or if the flow is turbulent a wall function can be used. It is therefore very easy to incorporate and test new ideas for improved wall functions in the context of deforming walls.

6.2 Pressure correction equations

The second condition (equation 41) will be used to derive an expression that links the pressure corrections on either side of the interface using the methodology presented in section 5.1. Taking the dot product of this equation with the normal vector $\vec{n}_s$ we have

$$-\frac{\lambda}{K} p_s + 2\mu \frac{\partial D_n}{\partial n_s} = -p_f + \left(t_{ij} \cdot n_{sj} \right) n_{si} \tag{42}$$

where p_s, p_f are the pressures on the solid and fluid side of the interface (see figure 1 for the notation).

The two pressures p_s, p_f are not equal i.e. there is a pressure jump. This can be made clearer with the aid of a simple example. Assume a circular cylinder subjected to internal gas pressure p_f while the external pressure is 0. The internal radius of the cylinder is r_i and its thickness is h, as shown in figure 2. The gas inside the cylinder is at rest so only the pressure force is acting on the internal cylinder wall. The cylinder has its axial end faces fixed i.e. the problem is plain strain. For this static case the analytic solution for all the stress components (i.e. radial, circumferential and axial) is known [25]. Using the definition of pressure for solids (equation 9) the value of p_s at the interface is evaluated from these stresses to be:

$$p_s = -\frac{2}{3}(1+\nu)\frac{p_f}{\left(\frac{r_i+h}{r_i}\right)^2 - 1} \tag{43}$$

It is obvious that $p_s \neq p_f$ and the pressure difference increases the thinner the cylinder is. Note also that the solid pressure is constant i.e. does not depend on the radius r. Of course, the normal stress (radial) is continuous. In fact, in order to obtain the analytic solution the boundary conditions $\sigma_{rr}(r_i) = -p_f$ and $\sigma_{rr}(r_i + h) = 0$ that express mathematically the continuity of radial stresses are employed. And of course this is exactly what equation 42 signifies in a more general setting.

The pressure and displacements must be corrected to satisfy this equation i.e.

$$-\frac{\lambda}{K}(p_s^* + p_s') + 2\mu\left(\frac{\delta D_n^*}{\delta n_s} + \frac{\delta D_n'}{\delta n_s}\right) + p_f^* + p_f' = (t_{ij} \cdot n_{sj}) n_{si} \tag{44}$$

Neglecting the contribution of the correction of normal displacement as before, we get

$$-\frac{\lambda}{K}p'_s + p'_f = \left(t_{ij}\cdot n_{sj}\right)n_{si} + \frac{\lambda}{K}p^*_s - 2\mu\frac{\partial D^*_n}{\partial n_s} - p^*_f \tag{45}$$

The right hand side of this equation is known. This expression provides the link between the pressure corrections on either side of the interface. Furthermore assuming that the pressure corrections at the boundary point (f) and the nearby centroid (F) on the fluid side are equal i.e. $p'_f = p'_F$ equation 45 can be solved for p'_s

$$p'_s = -\frac{K}{\lambda}\left(S_p - p'_F\right) \tag{46}$$

where $S_p = \left(t_{ij}\cdot n_{sj}\right)n_{si} + \frac{\lambda}{K}p^*_s - 2\mu\frac{\partial D^*_n}{\partial n_s} - p^*_f$ is known. This equation (which is the equivalent of 39 for fluid-structure interaction problems) will be used now to couple the pressure correction equations on the two sides together. For the evaluation of the interface normal velocity, the interpolation scheme proposed in [35] is used. However, due to pressure discontinuity at the interface, this scheme is applied on the solid side only i.e.

$$U^*_n = \overline{U^*_n} - DU_S\left(\frac{p^*_s - p^*_S}{\delta n} - \overline{\frac{\delta p^*}{\delta n}}\right) \tag{47}$$

where $DU_S = \frac{1}{2}\left(1 + \frac{\mu}{3K}\right)\frac{\Delta V_S}{A_P^{U_i}}$ and $\overline{U_n}$ is evaluated from linear extrapolation from the interior of the solid domain. In this way, derivatives of pressure across a discontinuity are avoided.

The pressure correction equation for the solid cell S next to the interface (see figure 1) is:

$$\frac{2\rho_S}{K_S}\frac{p^*_S + p'_S}{\Delta t}\cdot\Delta V_S + \left[\rho\left(U^*_i n_{si} - \frac{p'_s - p'_S}{\delta_s}DU_S\right)A\right]_s + \sum_{\substack{rest\ of\\ faces\ f}}\left[\rho\left(U^*_i + U'_i\right)n_i A\right]_f = S_m \tag{48}$$

Substituting p'_s from 46 and after some algebra we find that the discretised equation for pressure correction for cell S can be put on the form

$$A_P \cdot p'_S = A_F \cdot p'_F + \sum_{\substack{rest\ of \\ neighbours}} A_{nb} \cdot p'_{nb} + SU \tag{49}$$

where $A_F = \rho_s \frac{DU_S}{\delta_s} A_s \frac{K}{\lambda}$ while the contribution of the (s) face to the SU is $-\rho_s \frac{DU_S}{\delta_s} A_s \cdot \frac{K}{\lambda} S_p$ and to A_P is $\rho_s \frac{DU_S}{\delta_s} A_s$. Similarly, the pressure correction equation for the fluid cell F next to the interface (see figure 1) is

$$\frac{2\rho_F}{K_F} \frac{p_F^* + p'_F - p_F^{(k)}}{\Delta t} \cdot \Delta V_F + \left[\rho \left(U_i^* n_{fi} + \frac{p'_s - p'_S}{\delta_s} DU_S \right) A \right]_f + \sum_{\substack{rest\ of \\ faces\ f}} \left[\rho \left(U_i^* + U_i' \right) n_i A \right]_f = 0$$

(50)

Substituting p'_s from 46 and after some algebra the discretised equation for pressure correction for the fluid cell F can be put on the form

$$A_P \cdot p'_F = A_S \cdot p'_S + \sum_{\substack{rest\ of \\ neighbours}} A_{nb} \cdot p'_{nb} + SU \tag{51}$$

where $A_S = \rho_f \frac{DU_S}{\delta_s} A_f$ while the contribution of the (f) face to the SU is $\rho_f \frac{DU_S}{\delta_s} A_f \frac{K}{\lambda} S_p$ and to A_P is $\rho_f \frac{DU_S}{\delta_s} A_f \frac{K}{\lambda}$.

7. Results and discussion

The method described in the previous sections was implemented in an in-house three dimensional, fully unstructured, finite-volume code that solves for the three Cartesian components of velocity and pressure. The code has been used in the past to model successfully a variety of complex flow patterns [36-38]. For the fluid cells the equation set 18 was solved while for solids the system 22. For the convection terms the

2^{nd} order central differencing scheme was used. In order to accommodate the aforementioned pressure jump, the two media were detached at their interface and different values of pressure were stored at the fluid side and the solid side. Of course, the velocities and pressure corrections were solved simultaneously resulting in a strongly coupled velocity-pressure formulation for both media.

The method was applied to simulate the pressure wave propagation in an axisymmetric elastic tube. This is a standard problem that has been studied theoretically to a great extent (Atabek [39] among many others). However, the available analytic solutions for the displacement (radial and axial) and pressure are available on the frequency domain and are based on many simplified assumptions such as linearity of fluids equations, membrane equations for the solid wall etc. It was therefore decided to compare the results with the solution of the Flügge equations that account for the axial as well as bending stiffness of a thin shell. Details about the Flügge equations, the associated boundary conditions for the problem examined and their numerical solution are provided in Appendix A. More details on the assumptions employed for their derivation can be found in the book of Flügge [40]. These equations were coupled with the Navier-Stokes equations written in polar coordinates and were solved together using a separate in-house code.

The material properties for the solid and fluid component are shown in table 1. The fluid properties correspond to blood and were taken from Pedley [26]. The values of E and ν corresponding to human vessel walls are 10^6 and 0.5 respectively. A much higher value of E (2.2×10^{10}) was also examined in order to investigate the behaviour of the method for stiffer walls. The coordinate system employed as well as the basic dimensions and boundary conditions are shown in figure 3. The thickness of the tube is chosen deliberately to be small (1/20th of the tube radious) so that the theory of thin

shells can be applied. Computational details for the cases examined are provided in table 2. The pressure (in Pa) at the inlet increases linearly with time until a specified time instant T i.e.

$$p_{inl} = \begin{cases} 1000 \cdot \dfrac{t}{T} & (t \le T) \\ 1000 & (t > T) \end{cases} \tag{52}$$

The value of T (ramp time) is shown in table 2. Calculations with T=0 were also carried out to investigate the robustness of the method. The outlet pressure remained constant and equal to 0.

The computational domain was a slice of 5^o thickness with symmetry conditions on the two x-y planes. A zoomed-in isometric view of the three meshes examined close to the top boundary is depicted in figure 4.

For the values of E and ν equal to 10^6Pa and 0.3 respectively, the Flügge equations were solved twice using the same computational conditions (i.e. fluid mesh and time step) that were employed for the general solution method for cases 3 and 5, as shown in table 2. The results were almost identical and so the curves labelled "Flügge equations" for those values of E and ν were obtained using the coarse mesh 120x39 (case 3).

The variation of centreline pressure along the length of the pipe at 5 time instants is shown in figure 5. There are small differences between the predictions of the two meshes and the general agreement (especially for the fine mesh, case 5) with the Flügge equations is very good. Note that the peak pressure is higher compared to the maximum inlet pressure and this is predicted by both approaches. The speed of pressure wave propagation can be estimated by evaluating the distance travelled by the half-height of the maximum inlet pressure, i.e. 500Pa within a specified time interval. The propagation velocity in 4 successive time intervals of duration 2ms from 2ms-10ms is

found to be: 3.98m/s, 4.57m/s, 4.87m/s, 4.79m/s. The results with the Flügge equations are almost identical. It can be seen that the wave speed varies with the distance from the boundary end, which aggress with the theoretical finding of [41] for a semi-infinite tube. The smaller speed, especially in the first interval, might also be attributed to the linear increase of pressure with time at the inlet (equation 52).

For a tube of infinite length, one dimensional analysis [42] yields the following formula for the wave speed:

$$a = c_f \cdot \sqrt{\frac{K_f}{\rho_f} \cdot \left(1 + \frac{K_f}{E} \cdot \frac{D}{h} \cdot \left(1 - \nu^2\right)\right)^{-1}} \tag{53}$$

where K_f is the bulk modulus of the liquid, D is the internal pipe diameter and c_f is a factor that accounts for the axial stress waves in the pipe wall:

$$c_f^2 = 1 - \frac{\nu^2}{1 + \frac{E}{K_f}\frac{h}{D}\left(1 - \frac{K_f}{E}\frac{\rho_s}{\rho_f}\right)} \tag{54}$$

This expression is valid for a pipe allowed to expand or contract freely in its radial and axial directions with stress waves travelling in the pipe wall material in addition to the pressure waves propagating in the liquid [42]. The theoretically predicted value is 5.0m/s which agree very well (4% error or less) with the predicted values in the last two subintervals i.e. away from the inlet boundary where the pipe is free to deform in the axial as well as radial directions.

Contour plots of pressure for the 5 time instants are shown in figure 6. The pressure wave propagation is clearly seen as well as the areas of maximum pressure close to the wall behind the front. The pressure gradient induces an axial velocity at the inlet of the tube, whose variation along the centreline is shown in figure 7. The predictions between the present approach and the one using the Flügge equations are

almost identical. Superimposed is a horizontal line that represents the analytic expression from one dimensional analysis $V = \frac{\Delta p}{\rho_f \cdot \alpha}$ that gives a value of 0.20m/s. It is clear that when the pressure wave has fully developed after 2ms this value is closely approximated.

The variation of the radial displacement along the length of the tube for various meshes and time steps is presented in figure 8. The results for cases 1 and 2 (coarsest mesh) are shown only for the t=10ms to avoid cluttering up the figure. Clearly this mesh does not provide a grid-independent solution. The other two meshes provide results that are almost identical. Superimposed on the graph is the static radial displacement for a plain strain problem $w = \frac{\left(1-\nu^2\right) p_f \left(r_i + \frac{h}{2}\right)^2}{Eh}$ (where r_i is the internal radius of the pipe) which gives a value of 0.19mm. When the pressure pulse has propagated inside the pipe the value of radial displacement at the entrance approaches this value with good accuracy. Comparison between the Flügge equations using the finest mesh is shown in figure 9. There is excellent matching at the wave front where the radial displacement is smooth but in the wake of (i.e. behind) the front there are small differences in the maxima and minima between the two sets of results. These can be attributed to the assumptions inherent in the derivation of the Flügge equations as explained in the book of Flügge (1960). Calculations were also performed with membrane equations (obtained by setting $\beta = 0$ in equations A1, A2 in the Appendix A). The results (not shown here) again match very well in the area of smooth variation while behind the front the agreement with the present methodology was poorer compared to the Flügge equations. This is expected since close to the boundary the bending stiffness becomes important.

Figure 10 shows comparison of the axial displacement and again there is fairly good agreement between the two sets of results.

Calculations were also performed for an incompressible solid. A value of Poisson ratio equal to 0.5 exactly was used and the code converged is each time step without any stability problems. Comparison of pressure distribution for this case is shown in figure 11. The quality of matching between the two sets of results is similar as before.

In order to check the robustness of the method and code developed a calculation was carried out with the value of the ramp time T=0 (case 7 in table 2). Again the solid was incompressible. The convergence rate for this calculation at t=6ms is shown in figure 12. The underelaxation factors for both velocities and pressure were equal to 0.6 an no attempt was made to optimise them. The normalised residuals (which include both fluid and solid cells) drop by more than 6 orders of magnitude within about 20 iterations and the convergence is smooth and monotonous.

For all cases examined so far, the wave propagation velocity is determined by the compliance of the tube because $K_f >> E$. A final calculation (case 8 in table 2) was performed with a much stiffer wall (4 orders of magnitude larger modulus of elasticity), so both the compressibility of the liquid and the elasticity of the tube contribute to the wave speed. The pressure was recorded again at 5 time instances at intervals of 0.02ms i.e from 0-0.1ms. The predicted wave speeds were 620m/s, 625m/s, 628m/s, 623m/s, and match to within 3% the analytic solution (646m/s).

The previous results demonstrate the accuracy and the good performance of the proposed method. There is much scope for further development, for example by including large deformations, other constitutive equations for the solid material or by improving the convergence rate using a PISO-like approach. An advantage is that it can

be easily incorporated into existing CFD finite-volume codes as it is based on existing code philosophy and enlarge the range of problems that can be tackled without simplifying assumptions. The results presented in this paper deal only with laminar flows but extension to turbulent flows is straightforward. In this way, novel turbulence modelling ideas in the context of RANS or LES or novel wall functions can be tested in complex cases with moving boundaries where the deformation is determined by the solution of the flow field itself.

8. Conclusions

The paper presented a novel fully-coupled approach for modelling fluid-structure interaction problems for linear, elastic materials. It is based on a novel velocity-pressure formulation for both media and employs the same pressure-correction algorithm for the numerical solution of the set of partial differential equations. The method was applied to model the wave propagation in a flexible tube and comparison with existing analytic solutions or numerical results using the Flügge equations for a variety of cases showed very good performance. There is ample scope for the further development of the method to include large deformation, other materials and flow conditions.

.

References

[1] H.G. Matthies, J. Steindorf, Partitioned but strongly coupled iteration schemes for non-linear fluid-structure interaction problems, Comput. Struct. 80 (2002) 1991-1999.

[2] C. Farhat, M. Lesoinne, Two efficient staggered algorithms for the serial and parallel solution of three-dimensional nonlinear transient aeroelastic problems, Compu. Method Appl. M. 182 (2000) 499-515.

[3] A.K. Slone, K. Pericleous, C. Bailey, M. Cross, Dynamic fluid-structure interaction using finite volume unstructured mesh procedures, Comput. Struct. 80 (2002) 371-390.

[4] P. Le Tallec, J. Mouro, Fluid structure interaction with large structural displacements, Comput. Method Appl. M. 190 (2001) 3039-3067.

[5] H. T. Ahn, Y. Kallinderis, Strongly coupled flow/structure interactions with a geometrically conservative ALE scheme on general hybrid meshes, J. Comput. Phys. 219 (2006) 671-696.

[6] Y. Bazilevs, V.M. Calo, Y. Zhang, T.J.R. Hughes, Isogeometric fluid-structure interaction analysis with applications to arterial blood flow, Comput. Mech. 38 (2006) 310-322.

[7] M. Heil, An efficient solver for the fully coupled solution of large displacement fluid-structure interaction problems, Comput. Method Appl. M. 193 (2004) 1-23.

[8] T.E. Tezduyar, S. Sathe, K. Stein, Solution techniques for the fully discretised equations in computation of fluid-structure interactions with the space-time formulations, Comput. Method Appl. M. 195 (2006) 5743-5753.

[9] E. Oñate, M. Cervera, O.C. Zienkiewicz, A finite volume format for structural mechanics, Int. J. Numer. Meth. Eng. 37 (1994) 181-201.

[10] K. J. Bathe *Finite element procedures*, Prentice Hall, Englewood Cliffs, New Jersey, 1996.

[11] T.J.R. Hughes, *The finite element method: linear static and dynamic finite element analysis*, Dover Publications Inc., New York, 2000.

[12] P.M. Gresho, R.L. Sani, *Incompressible flow and the finite element method-volumes 1 and 2*, John Wiley and Sons, Chichester, 2000.

[13] C. Bailey, M. Cross A finite volume procedure to solve elastic solid mechanics problems in three dimensions on an unstructured mesh, Int. J. Numer. Meth. Eng. 38 (1995) 1757-1776.

[14] J.H. Ferziger, M. Peric, *Computational Methods for Fluid Dynamics*, Springer-Verlag, Berlin, Heidelberg, 1996.

[15] M.A. Wheel, A geometrically versatile finite volume formulation for plane elastostatic stress analysis, J. Strain Anal. Eng. 31 (1996) 111-116.

[16] M.A. Wheel, A mixed finite volume formulation for determining the small strain deformation of incompressible materials, Int. J. Numer. Meth. Eng. 44 (1999) 1843-1861.

[17] N.A. Fallah, C. Bailey, M. Cross, G.A. Taylor, Comparison of finite element and finite volume methods application in geometrically nonlinear stress analysis, Applied Math. Model. 24 (2000) 439-455.

[18] I. Demirdžic, S. Muzaferija, M. Peric, Benchmark solutions of some structural analysis problems using the finite-volume method and multigrid acceleration, Int. J. Numer. Meth. Eng. 40 (1997) 1893-1908.

[19] H. Jasak, H.G. Weller, Application of the finite volume method and unstructured meshes to linear elasticity, Int. J. Numer. Meth. Eng. 48 (2000) 267-287.

[20] C. Greenshields, H.G. Weller, A. Ivankovic, The finite volume method for coupled fluid flow and stress analysis, Comput. Model. Simulation Eng. 4(3) (1999) 213-218.

[21] A. Ivankovic, A. Karac, E. Dendrinos, K. Parker, Towards early diagnosis of atherosclerosis: the finite volume method for fluid-structure interaction, Biorheology 39 (2002) 401-407.

[22] C. Greenshields, H.G. Weller, A unified formulation for continuum mechanics applied to fluid-structure interaction in flexible tubes, Int. J. Numer. Meth. Eng. 64 (2005) 1575-1593.

[23] A. Karac, Drop Impact of fluid-filled polyethylene containers, PhD thesis, Dept. of Mechanical Engineering, Imperial College London, 2003.

[24] L.E. Malvern, *Introduction to the mechanics of a continuous medium*, Prentice-Hall Inc, New Jersey, 1969.

[25] W.M. Lai, D. Rubin, E. Krempl, *Introduction to continuum mechanics*, 3rd edition, Butterworth-Heinemann, Massachusetts, 1996.

[26] T.J. Pedley, *The fluid mechanics of large blood vessels*, Cambridge University Press, Cambridge, 1980.

[27] A.E. Vardy, A.T. Alsarraj, Method of characteristics analysis of one-dimensional members, J. Sound Vib. 129 (1989) 477-487.

[28] X. Lin, J. Ballman, A numerical scheme for axisymmetric elastic waves in solids, Wave Motion 21 (1995) 115-126.

[29] G. Giese, M. Fey, A genuinely multidimensional high-resolution scheme for the elastic-plastic wave equation, J. Comput. Phys. 181 (2002) 338-353.

[30] P. Voinovich, A. Merlen, Two-dimensional unstructured elastic model for acoustic pulse scattering at solid-liquid interfaces, Shock Waves 13 (2003) 421-429.

[31] R. J. LeVeque, *Finite volume methods for hyperbolic problems*, Cambridge University Press, Cambridge, 2002.

[32] S. Patankar, *Numerical Heat Transfer and Fluid Flow*, Hemisphere Publishing Corporation, Washington, 1980.

[33] H.K.Versteeg, W. Malalasekera, *An Introduction to Computational Fluid Dynamics; The finite Volume method*, 2nd edition, Pearson Education Limited, Harlow England, 2007.

[34] R. I. Issa, Solution of the implicit discretised fluid flow equation by operator-splitting, J. Comput. Phys. 62 (1986) 40-65.

[35] C.M. Rhie, W.L. Chow, A numerical study of the turbulent flow past an isolated airfoil with trailing edge separation, AIAA J. 21 (1983) 1525-1532.

[36] S.L. Yeoh, G. Papadakis, M. Yianneskis, Determination of mixing time and degree of homogeneity in stirred vessels with LES, Chem. Eng. Sci. 60 (2005) 2293-2302.

[37] C. Liang, G. Papadakis, Large Eddy Simulation of pulsating cross-flow over a circular cylinder at subcritical Reynolds number, Comput. Fluids 36 (2007a) 299-312.

[38] C. Liang, G. Papadakis, Large eddy simulation of cross flow through a staggered tube bundle at subcritical Reynolds number, J. Fluid Struct. 23 (2007b) 1215-1230.

[39] H.B. Atabek, Wave propagation through a viscous fluid contained in a tethered, initially stressed, orthotropic elastic tube, Biophys. J. 8 (1968) 626-649.

[40] W. Flügge, *Stresses in shells*, Springer-Verlag, Berlin, Heidelberg, 1960.

[41] G.D.C. Kuiken, Wave propagation in a thin-walled liquid-filled initially stressed tube, J. Fluid Mech. 141 (1984) 289-308.

[42] S. Struckenbruck, D.C. Wiggert, R.S. Otwell, The influence of pipe motion on acoustic wave propagation, J. Fluids Eng.- Trans. ASME, 107 (1985) 518-522.

[43] A.C. Ugural, *Stresses in plates and shells*, 2nd Edition, Mc-Graw Hill, Singapore, 1999.

Appendix A: The Flügge equations and their numerical solution.

The equations of Flügge (1960) extend the basic membrane equations by accounting for the bending stiffness of thin shells. For axisymmetric conditions, the axial and radial momentum equations are

$$\gamma \frac{\partial^2 u}{\partial t^2} = u'' + \nu w' - \beta w'' \tag{A1}$$

and

$$-\gamma \frac{\partial^2 w}{\partial t^2} = w + \nu u' + \beta\left(w'''' - u''' + w\right) - p_f \frac{a^2}{D} \tag{A2}$$

respectively where $(\ )' = a\frac{\partial(\ )}{\partial x}$ and the parameters β, γ, D are defined as

$$\begin{aligned} \beta &= \frac{1}{12}\left(\frac{h}{a}\right)^2 \\ \gamma &= \rho \frac{1-\nu^2}{E} a^2 \\ D &= \frac{Eh}{1-\nu^2} \end{aligned} \tag{A3}$$

In the above equations, a is the radius of the middle surface, u is its axial displacement, w its radial displacement (positive along increasing radius) and h the thickness of the shell. The terms that account for flexural rigidity (bending stiffness) are the ones multiplied by the parameter β. For $\beta = 0$ the equations reduce to the membrane equations used widely for the theoretical analysis of pulse propagation in flexible tubes. The value of the radial displacement velocity $\left(\frac{\partial w}{\partial t}\right)$ is used as boundary condition for the solution of the Navier-Stokes and continuity equations in axisymmetric coordinates. The boundary condition for equation A1 is

$$u = 0 \tag{A4}$$

on either end of the solid domain. Since the equation A2 is 4th order, 2 boundary conditions are needed at each end. For the sliding edge, these conditions are

$$w''' = u''$$
$$w' = 0 \qquad \text{(A5)}$$

The first expresses mathematically the fact that the shear stress is 0 and the second that rotation is prevented.

The above equations were discretised using the finite difference method. Standard central difference approximations were employed to approximate the 2nd, 3rd and 4th order derivatives at the interior of the domain [43] i.e. for values of i=2…ni-1 (see figure A1). The standard expressions for uniform mesh were modified close to the boundaries to account for the varying distances between the points.

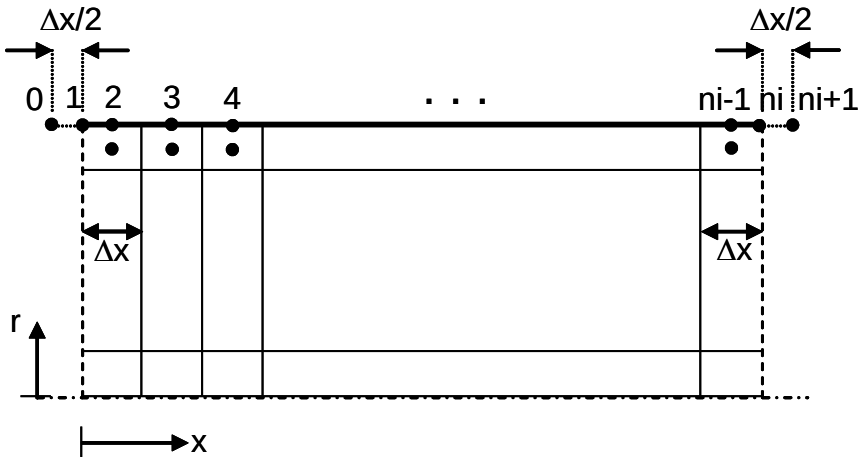

Figure A1. Sketch of computational domain and auxiliary points at the ends.

The implementation of the boundary condition A4 for the left end of the domain is straightforward:

$$u_1 = 0 \qquad \text{(A6)}$$

However A5 is more involved. The 3rd order derivative was discretised at point i=1 with the help of the auxiliary point i=0, located a distance Δx/2 on the left of point 1 i.e.

symmetrical to point 2. For the 2nd order derivative a forward approximation was used. Taking into account the different distances between the various points the discretised form of equations A5 is:

$$\begin{aligned} a^3 \frac{2\left(w_3 - 6w_2 + 8w_1 - 3w_0\right)}{\Delta x^3} &= a^2 \frac{4}{3} \frac{u_3 - 3u_2 + u_1}{\Delta x^2} \\ a \frac{w_2 - w_0}{\Delta x} &= 0 \end{aligned} \tag{A7}$$

The value of w_0 can be evaluated from the second of A7 therefore we have:

$$a \frac{w_3 - 9w_2 + 8w_1}{\Delta x} = \frac{2}{3}\left(u_3 - 3u_2\right) \tag{A8}$$

in which A6 was used. This equation provides an implicit expression for w_1 which is used as Dirichlet boundary condition:

$$w_1 = \frac{1}{8}\left(\frac{2\Delta x}{3a}\left(u_3 - 3u_2\right) + 9w_2 - w_3 \right) \tag{A9}$$

The treatment of the right boundary is identical.

Figure captions

Figure 1 Two cells on either side of the interface.

Figure 2 A cylinder subjected to internal gas pressure

Figure 3 Sketch of the computational domain with basic dimensions (in mm) and boundary conditions.

Figure 4 Isometric views of the 3 meshes zoomed-in at the top boundary.

Figure 5 Variation of centreline pressure at 5 time instants.

Figure 6 Pressure contours at 5 time instants.

Figure 7 Variation of centreline axial velocity at 5 time instants.

Figure 8 Predicted radial displacement with various meshes and time steps (Cases 1-5).

Figure 9 Predicted radial displacement and comparison with Flügge equations.

Figure 10 Predicted axial displacement and comparison with Flügge equations.

Figure 11 Predicted pressure distribution and comparison with Flügge equations for an incompressible solid.

Figure 12 Convergence history for case 7.

Table 1. Physical properties of the solid and fluid materials

Solid properties	
Modulus of Elasticity (Pa)	10^6, $2.2x10^{10}$
Poisson ratio (-)	0.3, 0.5
Density (Kg/m^3)	1000
Fluid properties	
Dynamic viscosity (Ns/m^2)	0.004
Density (Kg/m^3)	1000
Bulk modulus (Pa)	$2.2x10^9$

Table 2. Computational details for the cases examined. A tick "√" in the "Solution of the Flügge equations" column for a particular case signifies that these equations were also solved using the same computational conditions (i.e. fluid mesh size and time step) employed in the general solution method for that case.

Case number	Mesh size $ny \times (nx_f + nx_s)^*$	Δt (s)	Ramp Time (s)	Poisson ratio	Modulus of elasticity (Pa)	Solution of Flügge equations
1	60x(19+5)	$2x10^{-5}$	$2x10^{-3}$	0.3	10^6	-
2	60x(19+5)	$4x10^{-6}$	$2x10^{-3}$	0.3	10^6	-
3	120x(39+10)	$4x10^{-6}$	$2x10^{-3}$	0.3	10^6	√
4	120x(39+10)	10^{-6}	$2x10^{-3}$	0.3	10^6	-
5	180x(59+10)	10^{-6}	$2x10^{-3}$	0.3	10^6	√
6	120x(39+10)	10^{-6}	$2x10^{-3}$	0.5	10^6	√
7	120x(39+10)	10^{-6}	0	0.5	10^6	-
8	120x(39+10)	10^{-7}	$2x10^{-5}$	0.3	$2.2x10^{10}$	-

* ny is the number of cells in the y direction and nx_f ,nx_s are the number of cells in the x direction for the fluid and solid medium respectively.

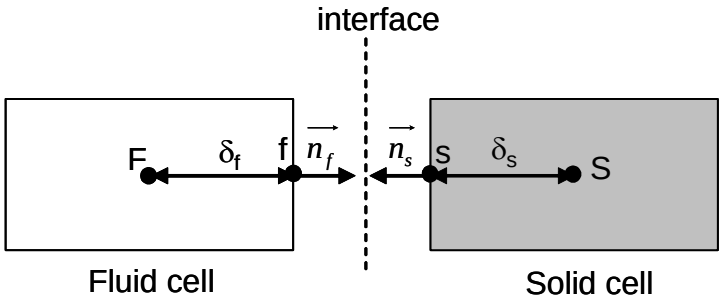

Figure 1 Two cells on either side of the interface.

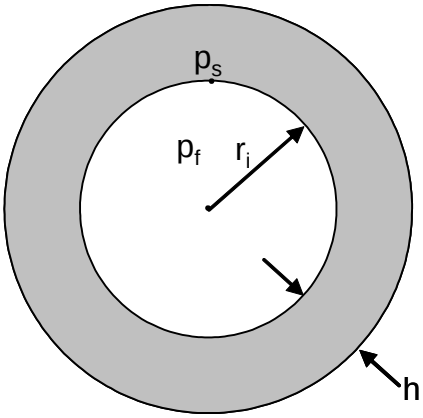

Figure 2 A cylinder subjected to internal gas pressure

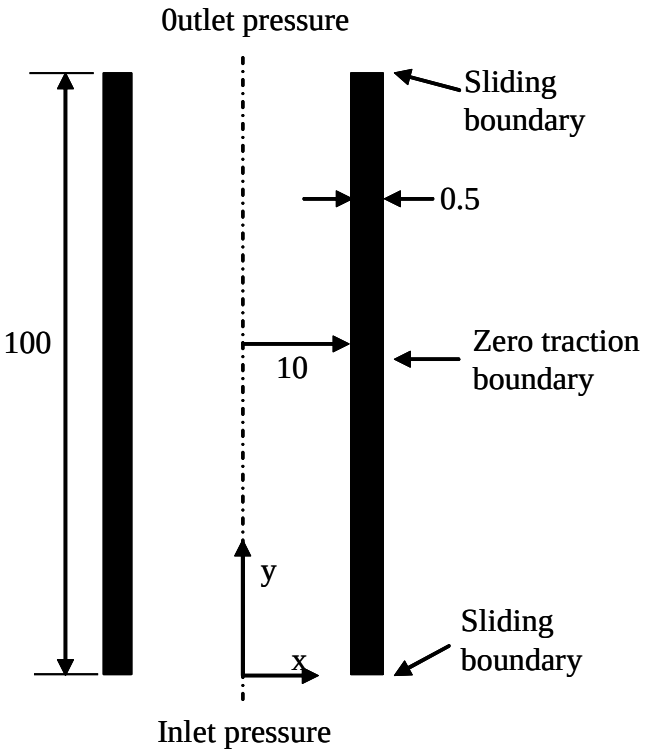

Figure 3 Sketch of the computational domain with basic dimensions (in mm) and boundary conditions.

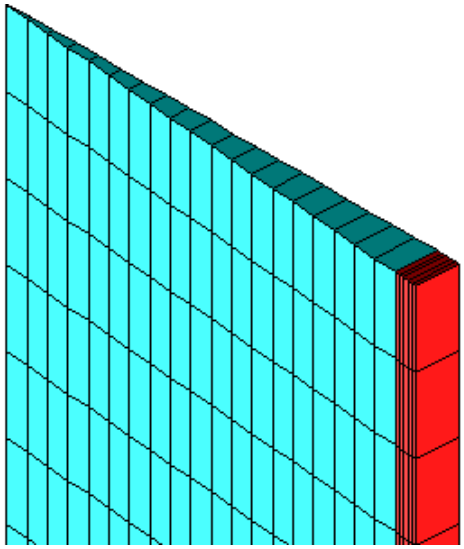

(a) Mesh 60x(19+5)

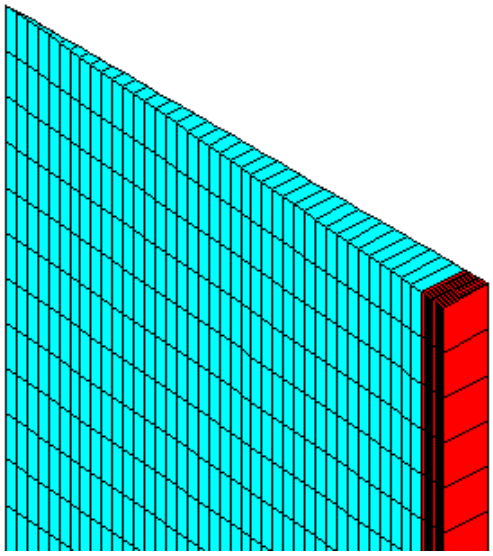

(b) Mesh 120x(39+10)

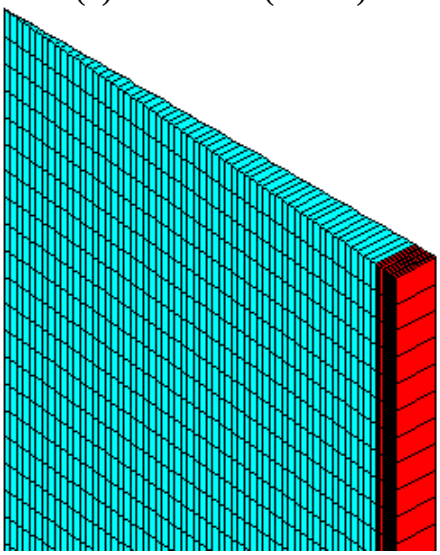

(c) Mesh 180x(59+10)

Figure 4 Isometric views of the 3 meshes zoomed-in at the top boundary.

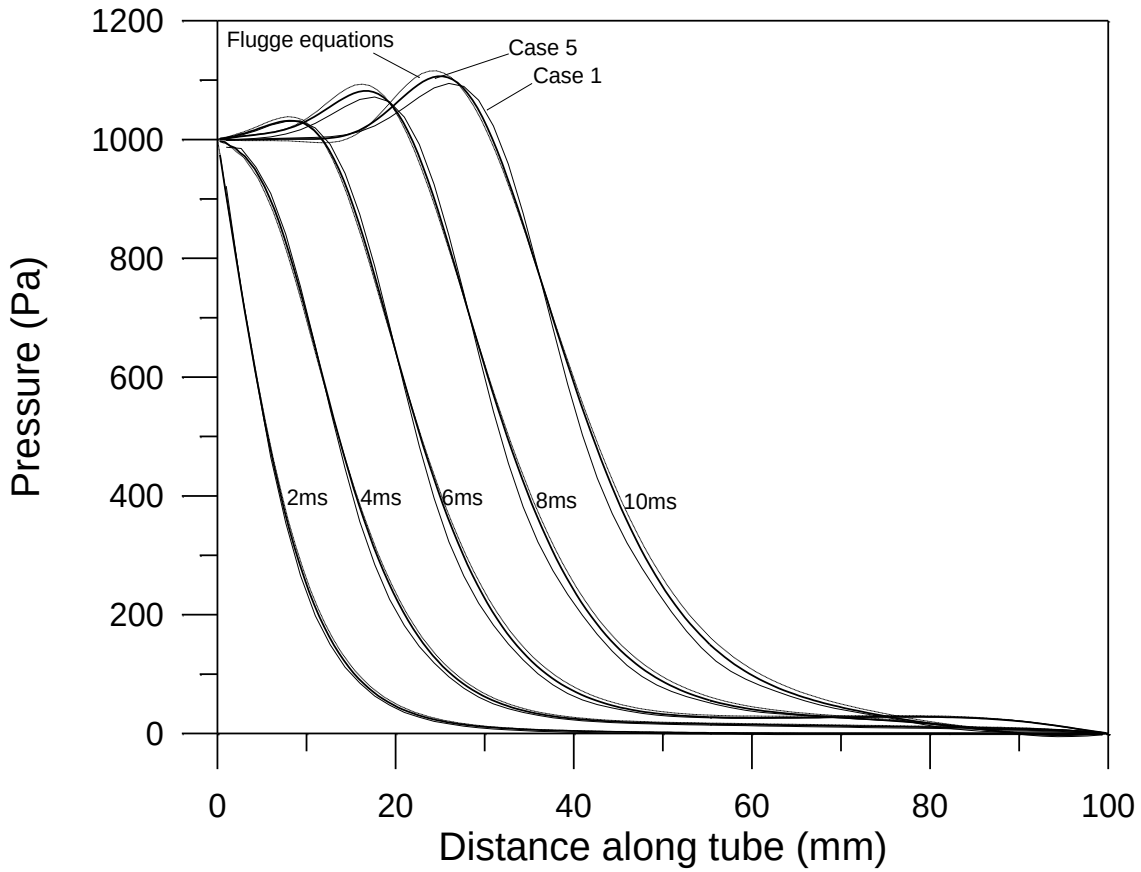

Figure 5 Variation of centreline pressure at 5 time instants.

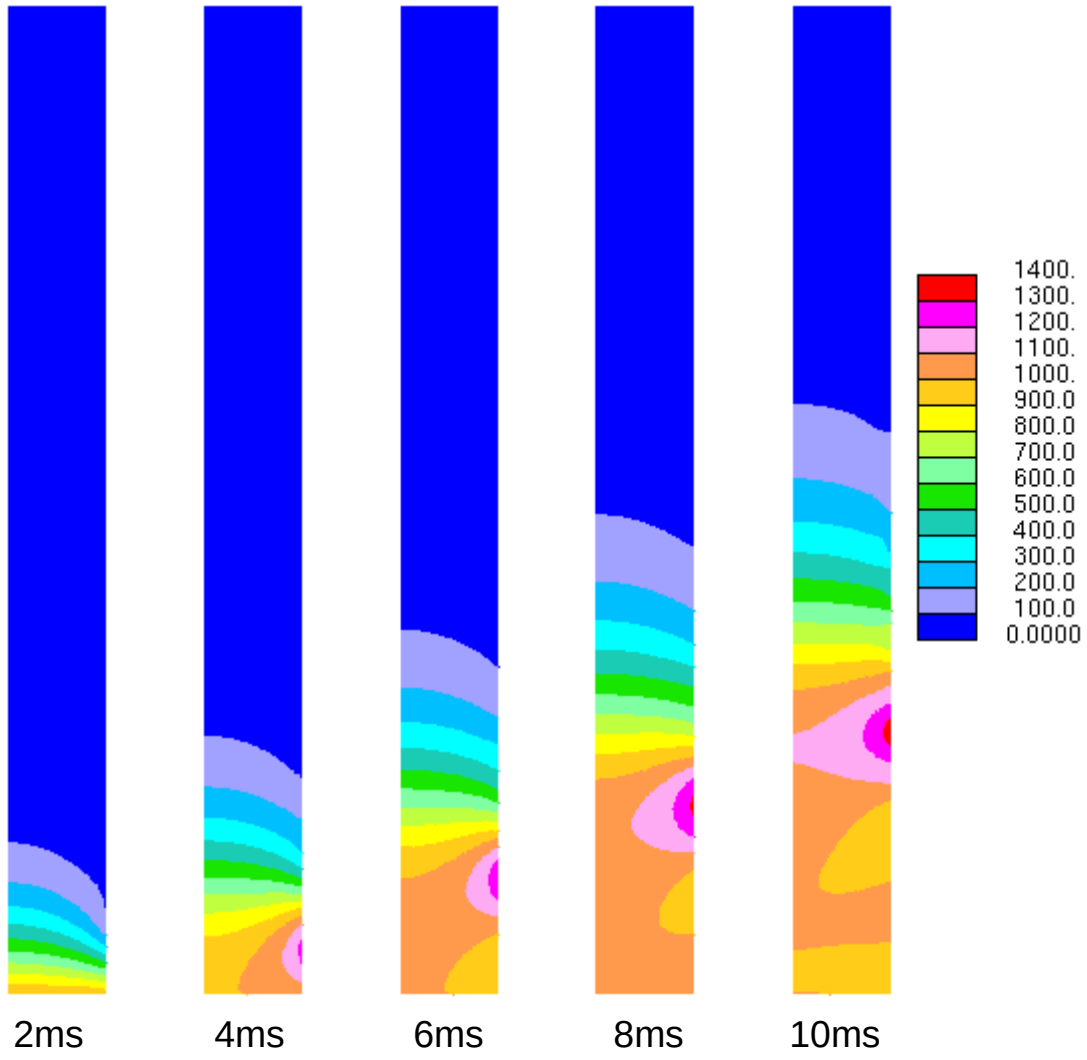

Figure 6 Pressure contours at 5 time instants.

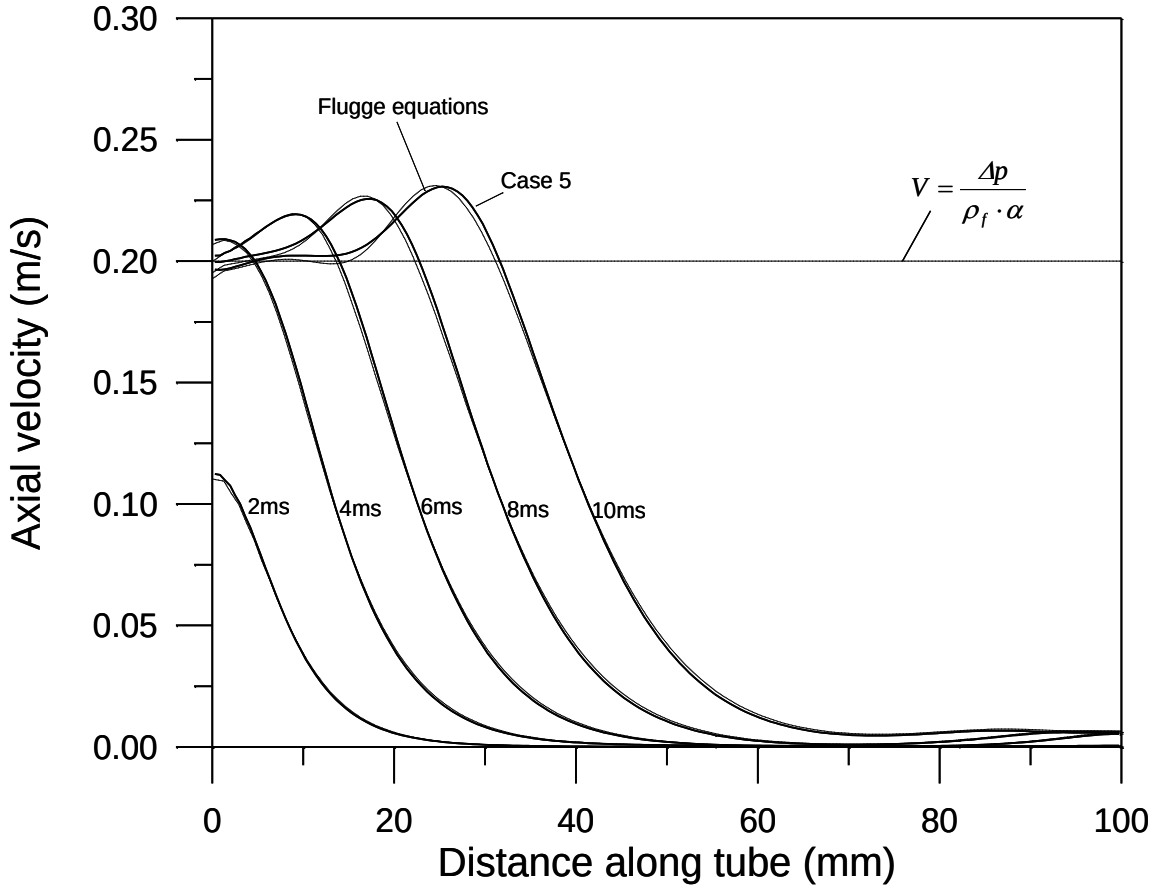

Figure 7 Variation of centreline axial velocity at 5 time instants.

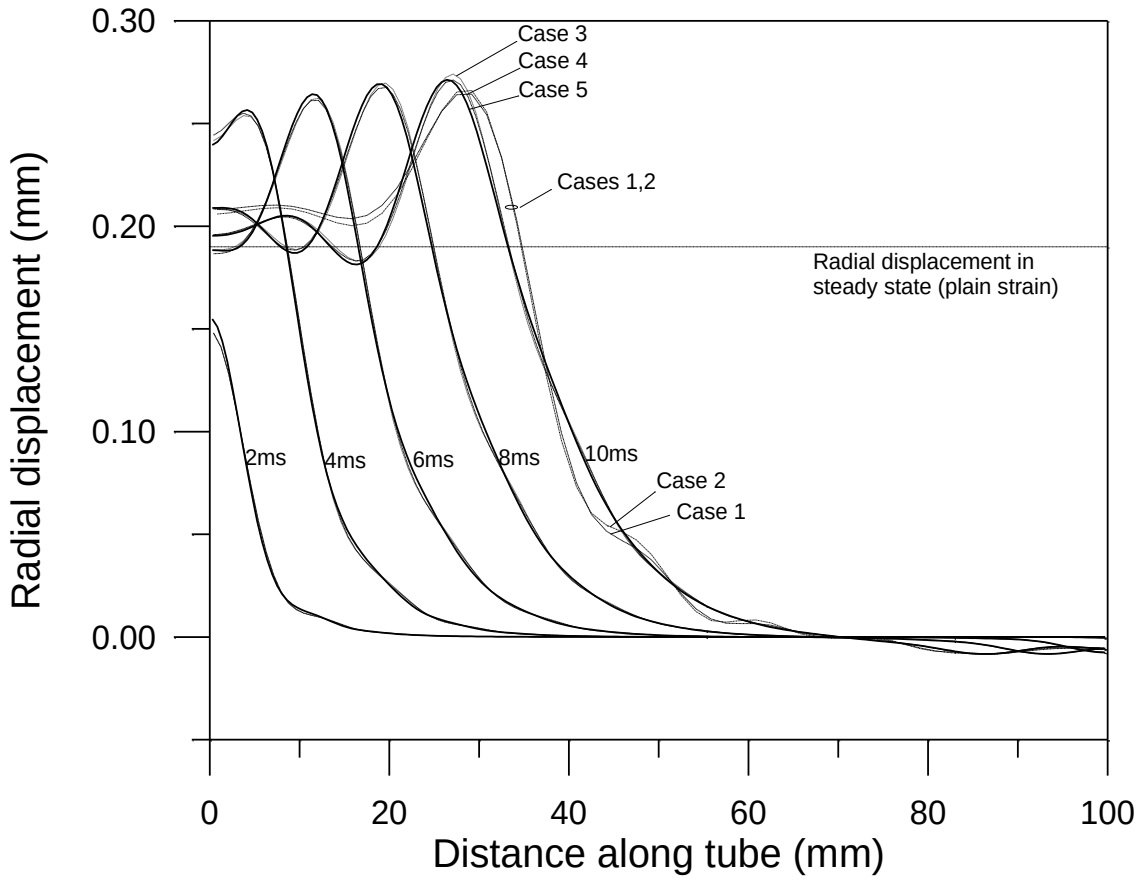

Figure 8 Predicted radial displacement with various meshes and time steps (Cases 1-5).

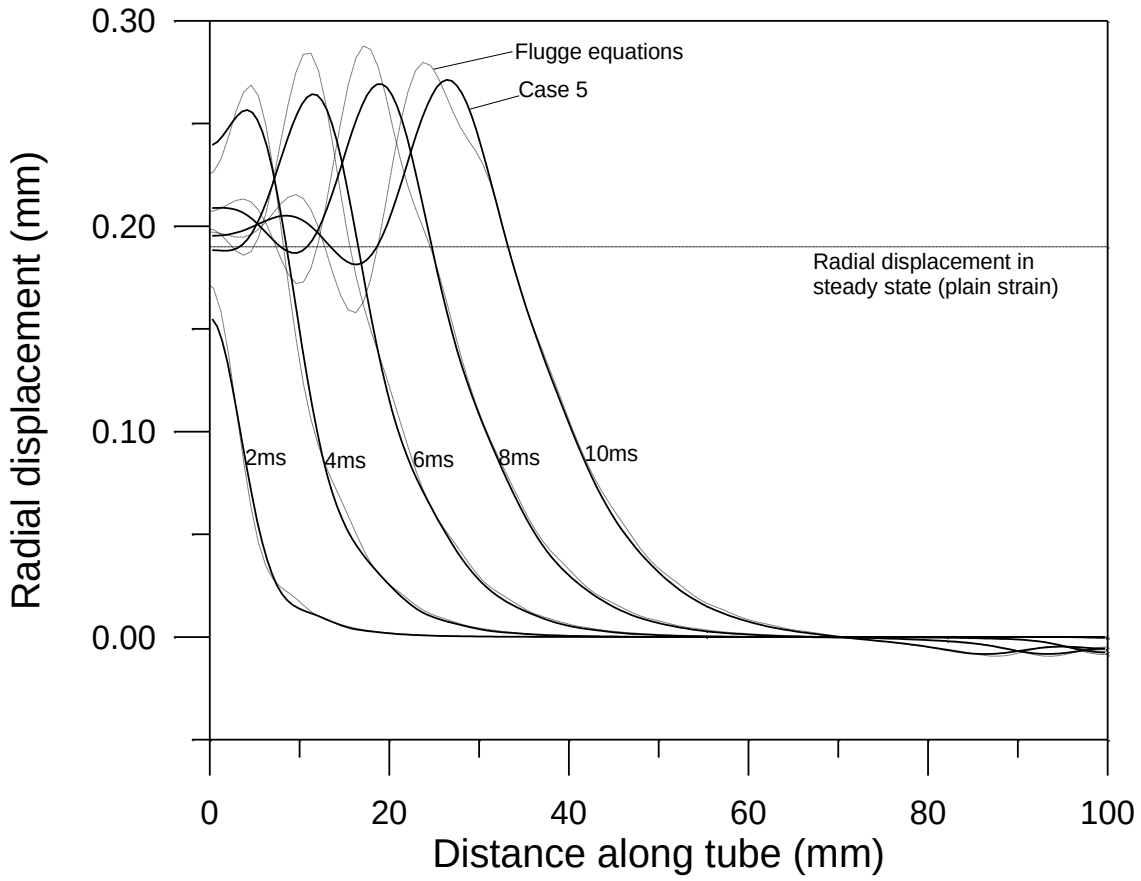

Figure 9 Predicted radial displacement and comparison with Flügge equations.

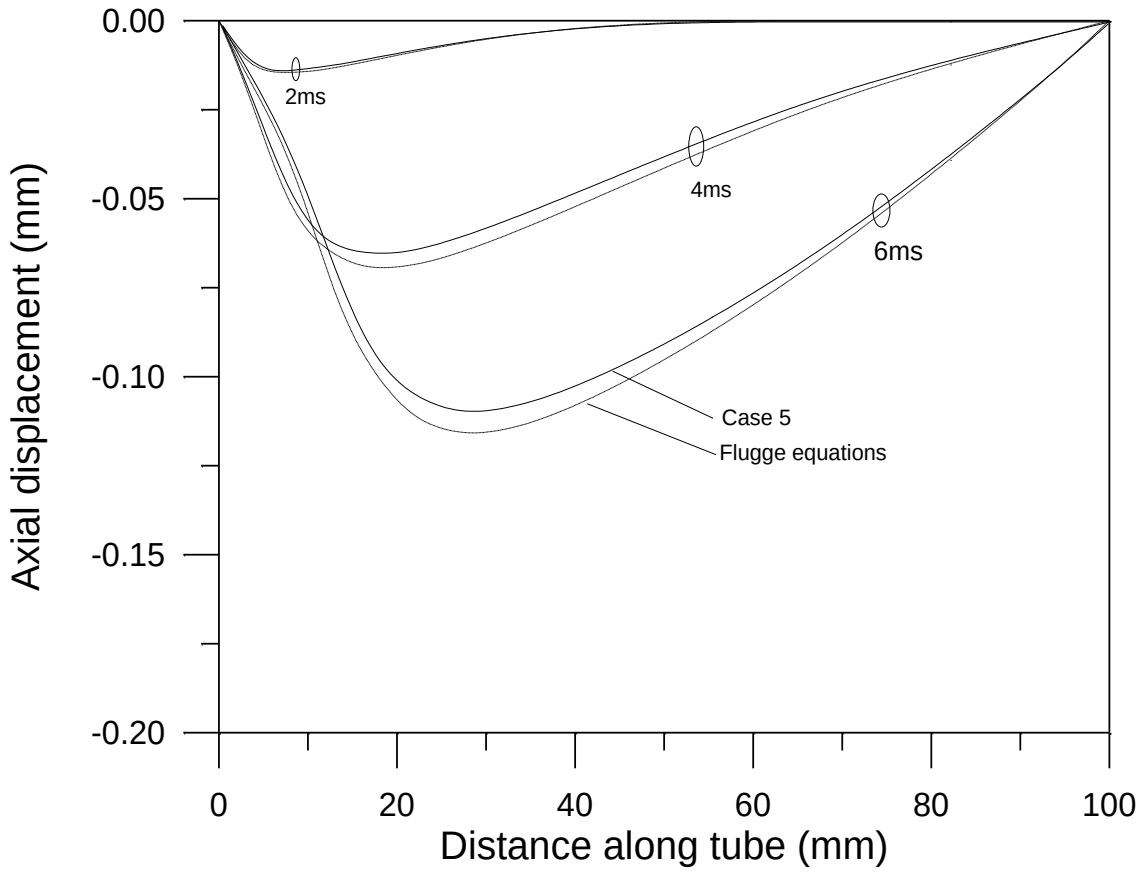

Figure 10 Predicted axial displacement and comparison with Flügge equations.

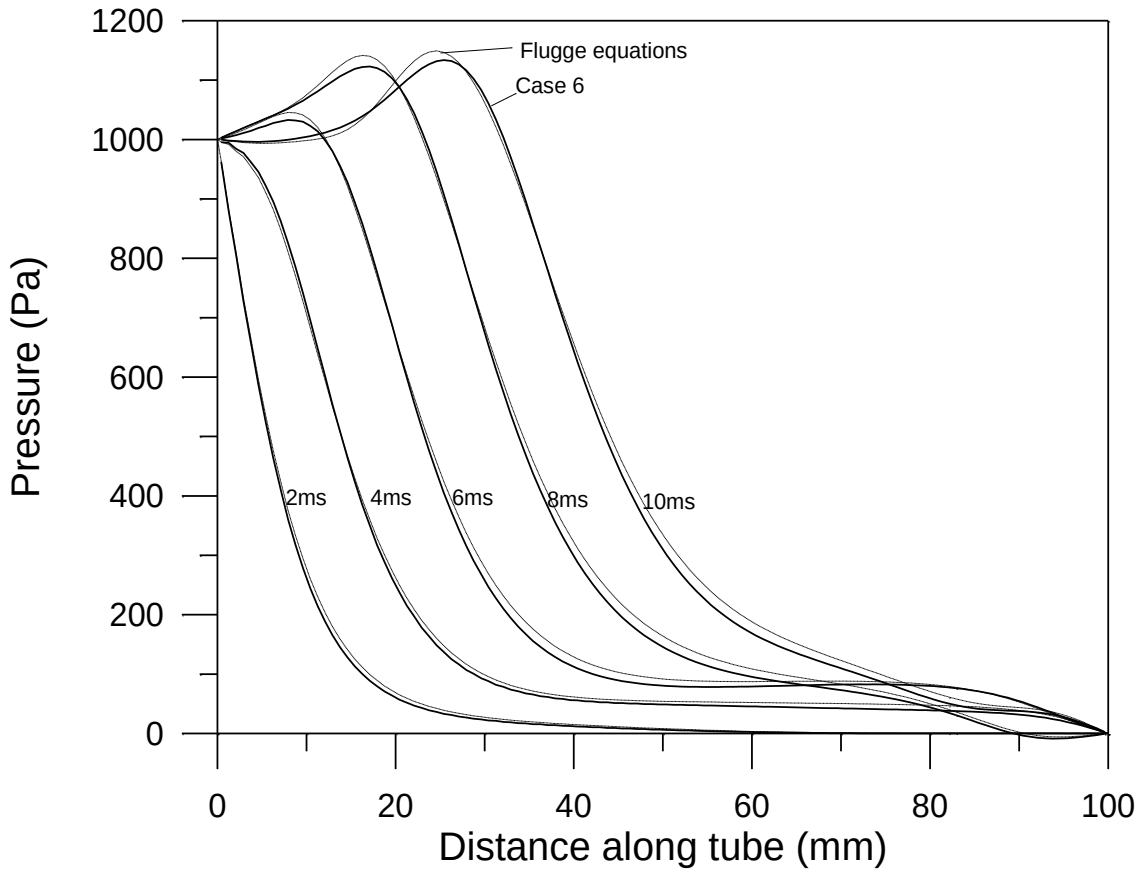

Figure 11 Predicted pressure distribution and comparison with Flügge equations for an incompressible solid.

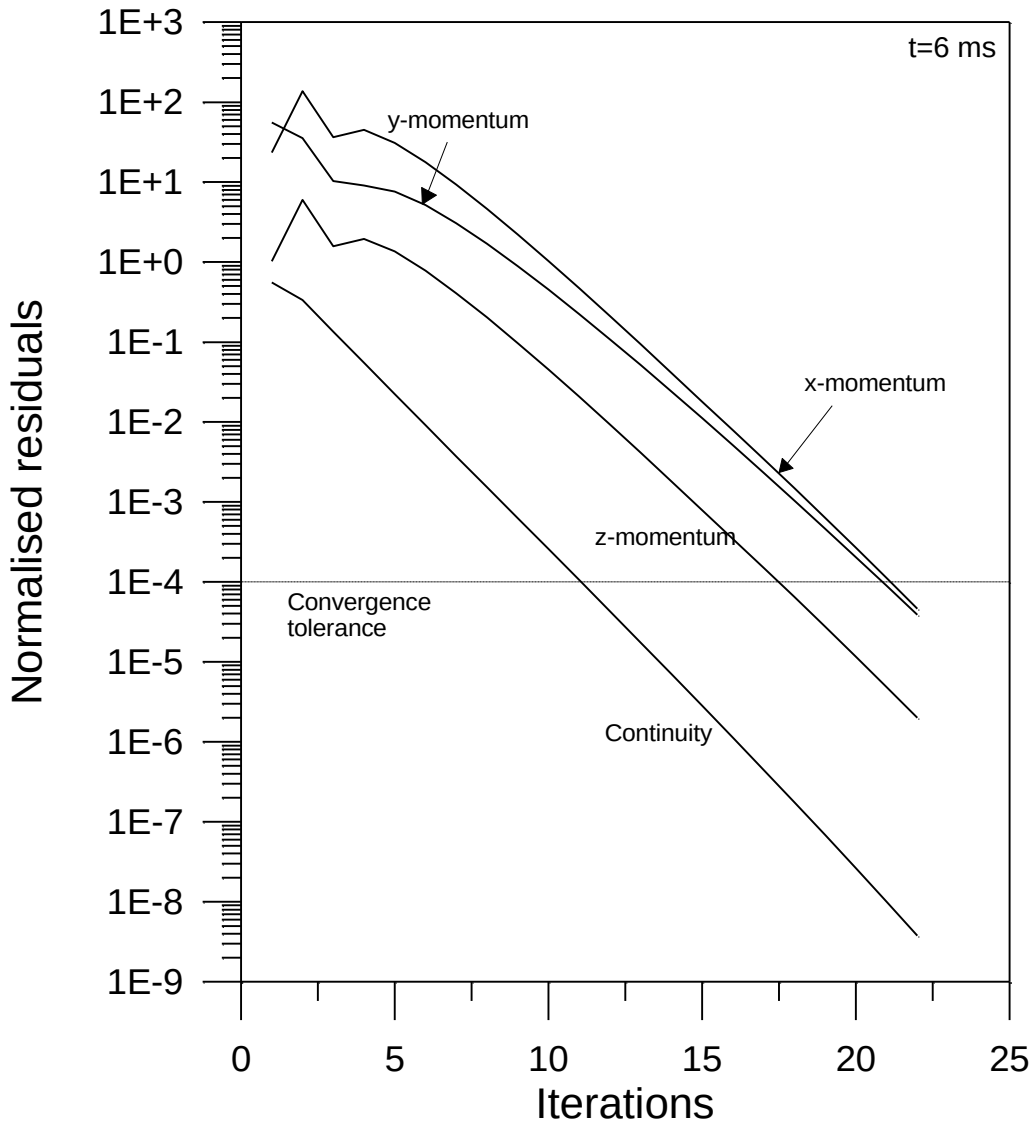

Figure 12 Convergence history for case 7.